NON TRADITIONAL GYRO-BASED EKF FOR SMALL SATELLITE ATTITUDE ESTIMATION AND SENSOR BIAS CALIBRATION

Hasan Kinatas[1)], Chingiz Hajiyev[2)]
[1), 2)] *Aeronautics and Astronautics Faculty, Istanbul Technical University, Istanbul, Turkey*
[1)] kinatas16@itu.edu.tr, [2)] cingiz@itu.edu.tr

This study proposes a non traditional gyro-based estimation system for attitude estimation and sensor bias calibration of a small satellite. The proposed system combines the TRIAD algorithm, a vector based attitude determination method, with an extended Kalman filter (EKF) in order to reduce the computational load and bring flexibility to the filter. As the first step, the TRIAD algorithm produces an initial coarse quaternion set estimation using three-axis magnetometer and sun sensor measurements. Then, this coarse estimation is filtered to obtain the final estimation. Besides attitude estimation, EKF also helps to correct the magnetometer and gyroscope measurements by estimating the corresponding bias vectors. In order to verify the performance of the proposed system, several numerical simulations are performed for a hypothetical nanosatellite. Simulations include attitude, magnetometer bias, and gyro bias estimation results as well as the performance of the proposed system in different angular velocities and for various time-varying magnetometer biases.

Key Words: Small satellites, attitude estimation, sensor calibration, Kalman filtering, magnetometers, time-varying bias

1. Introduction

In recent years, small satellites, especially nanosatellites, have attracted significant attention, both in industry and in academia[1)]. Their low cost and short development time have prompted more people and private companies to work in the field of satellite technologies. However, such satellites, which are strictly limited in terms of mass, size and cost, also bring some difficulties in the development and design phases. The use of expensive and high-capability components may not be possible due to cost constraints, or the number of sensors that can be used may have to be limited due to size and mass constraints. The attitude determination & control subsystem (ADCS) is one of the most important subsystems on a satellite and is also one of the most affected by the on-orbit spacecraft failures together with the orbit control subsystem[2)]. Having an on-board computer with limited computational power and the use of commercial off-the-shelf (COTS) sensors and actuators due to above mentioned limitations make the design of this subsystem especially a challenging task for nanosatellites. Focusing on the attitude determination part, it is expected that the designed system should be able to quickly estimate the attitude within a predetermined accuracy range and at the same time not require much computational power.

The traditional approach to attitude estimation algorithms for spacecrafts in general includes the use of an extended or unscented Kalman filter (EKF or UKF)[3-7)]. However, these approaches may require large amounts of computational power due to the non-linearity of the measurement models of some of the attitude sensors (e.g., magnetometer) and thus may not be practical for small satellites. One of the ways to deal with this non-linearity in measurement models is to preprocess the sensor measurements using one of the static attitude determination methods (e.g., TRIAD, QUEST, SVD) and obtain an initial attitude estimation which then can be fed to the filter. These approaches are known as the integrated or non-traditional approaches and numerous studies on the subject are available[8-11)]. Direct input of the attitude information makes the measurement model for the filter linear since the states become directly observable and thus partially reduces the computational load. Another advantage of these methods is that they are more flexible than traditional filtering, as switching between different attitude sensors is easier.

Besides the computational load, another issue to consider during the design phase of the attitude estimation algorithm for small satellites is the error proneness of COTS attitude sensors. In particular, magnetometers, which are indispensable components of basic small satellite sensor packages, are affected by many different types of errors such as biases, scale factors, and non-orthogonality in magnetometer axes[12)]. Since a magnetometer with these errors will not be able to provide accurate measurements, it must be in-flight calibrated to achieve higher accuracy in attitude estimation. The survey paper[13)] presents a comprehensive study of magnetometer calibration methods including attitude-dependent, attitude-independent, sequential, and batch calibration. In this study, the use of the Kalman filter for calibration falls under the attitude-dependent sequential calibration category, and there are studies in the literature that present complete magnetometer calibration with this method[14-16)].

Another important component of the small satellite ADCS are gyroscopes. Although not directly an attitude sensor, they are used to propagate satellite kinematics during filtering as they provide angular velocity measurements to the system. Filters in which kinematic equations are propagated in this way are known as gyro-based filters and in these filters, gyro biases are also estimated in addition to the attitude[17)]. Another approach to attitude filtering is to propagate the satellite kinematics using the satellite dynamics, which filters using this approach are known as dynamics-based filters. However, in

practice it is impossible to build a perfect dynamic model for a satellite, which leads to more frequent use of gyro-based filters. There are also studies that make use of both dynamic model and gyroscope measurements[7,18]. This method, in which attitude, angular velocity and gyroscope biases are estimated simultaneously, can be particularly advantageous when there are uncertainties in both the gyroscope measurements and the dynamic model.

In this study, an integrated TRIAD/EKF system is proposed for attitude estimation, and magnetometer and gyro bias calibration of a small satellite. The TRIAD algorithm is used as the first stage attitude determination method since it is computationally less demanding compared to other methods, which is an important requirement for a small satellite. Since it is very difficult to model realistically, satellite dynamics was not exploited throughout the study and therefore the system can be considered as a gyro-based system. In order to verify the performance of the system, several numerical simulations are performed for a hypothetical nanosatellite. Apart from the estimation results and accuracy, these simulations also include the performance of the system in different angular velocities and for various time-varying magnetometer biases. Although there are studies in existing literature proposing similar systems using a UKF[19,20], this study discusses the use of an EKF in a non-traditional way for time-varying magnetometer bias estimation which has not been discussed in any of previous publications.

2. Small Satellite Attitude Kinematics and Sensor Measurement Models

2.1. Satellite Attitude Kinematics

The quaternion-based satellite attitude kinematics equation is given in the compact form as[12]

$$\dot{\boldsymbol{q}} = \frac{1}{2}\Omega(\boldsymbol{\omega}_{br})\boldsymbol{q} \tag{1}$$

where $\boldsymbol{q}$ is the four component quaternion vector and $\boldsymbol{\omega}_{br}$ is the body angular velocity vector with respect to the reference frame. $\Omega(\cdot)$ symbol represents the skew-symmetric matrix and for $\boldsymbol{\omega}_{br}$, it is defined as

$$\Omega(\boldsymbol{\omega}_{br}) = \begin{bmatrix} 0 & \omega_{br_z} & -\omega_{br_y} & \omega_{br_x} \\ -\omega_{br_z} & 0 & \omega_{br_x} & \omega_{br_y} \\ \omega_{br_y} & -\omega_{br_x} & 0 & \omega_{br_z} \\ -\omega_{br_x} & -\omega_{br_y} & -\omega_{br_z} & 0 \end{bmatrix} \tag{2}$$

Here, it should be noted that Eq. (1) is highly dependent on the chosen reference frame. For gyro-based filters (as in this study), satellite kinematics are propagated using gyroscope measurements, which are devices measuring the body angular velocity with respect to the inertial frame. If the reference frame is chosen as the Earth-centered inertial (ECI) frame, then gyroscope measurements can be used directly in Eq. (1). However, if the chosen reference is not an inertial frame, then angular velocity measurements should be transformed accordingly. In this study, the orbital frame is chosen as the reference frame. Therefore, a transformation is needed as follows

$$\boldsymbol{\omega}_{br} = \boldsymbol{\omega}_{bo} = \tilde{\boldsymbol{\omega}}_{bi} - A[0 \quad -\omega_o \quad 0] \tag{3}$$

where $\boldsymbol{\omega}_{bo}$ is the body angular velocity vector with respect orbital frame, $\tilde{\boldsymbol{\omega}}_{bi}$ is the gyroscope measurement, A is the attitude matrix, and ω_o is the angular velocity of the orbit which can be obtained for a circular orbit as

$$\omega_o = \sqrt{\frac{\mu}{r_0^3}} \tag{4}$$

where μ is the gravitational parameters and r_0 is the distance between the center of mass of the satellite and the Earth.

2.2. Sensor Measurement Models

The proposed system uses a three-axis magnetometer and a sun sensor as the attitude sensors, and also has a gyroscope that provides body angular velocity measurements for the satellite kinematics. The magnetometer measurement model including sensor noise and bias can be given as follows

$$\tilde{\boldsymbol{B}}_b = A\boldsymbol{B}_r + \boldsymbol{\eta}_m + \boldsymbol{b}_m \tag{5}$$

where $\tilde{\boldsymbol{B}}_b$ is the measured magnetic field vector in body frame, $\boldsymbol{B}_r$ is the magnetic field vector in reference frame, $\boldsymbol{b}_m$ is the bias vector, and $\boldsymbol{\eta}_m$ is the sensor noise vector which is assumed to be a zero-mean white Gaussian noise. The behavior of magnetometer bias vector, on the other hand, is given by

$$\frac{\mathrm{d}\boldsymbol{b}_\mathrm{m}}{\mathrm{dt}} = \boldsymbol{\eta}_{\mathrm{m,b}} \tag{6}$$

where $\boldsymbol{\eta}_{m,b}$ is the bias noise vector which is assumed to be a zero-mean white Gaussian noise.

The Earth magnetic field vector $\boldsymbol{B}_r$ can be modeled in orbital frame using the International Geomagnetic Reference Field (IGRF) model[21] with a dipole approximation[15] as

$$B_{r_x} = \frac{M_e}{r_0^3}\{c(\omega_o t)[c(\varepsilon)s(i) - s(\varepsilon)c(i)c(\omega_e t)] - s(\omega_o t)s(\varepsilon)s(\omega_e t)\} \tag{7}$$

$$B_{r_y} = -\frac{M_e}{r_0^3}\{c(\varepsilon)s(i) + s(\varepsilon)s(i)c(\omega_e t)\} \tag{8}$$

$$B_{r_z} = \frac{2M_e}{r_0^3}s(\omega_o t)[c(\varepsilon)s(i) - s(\varepsilon)c(i)c(\omega_e t)] - 2s(\omega_o t)s(\varepsilon)s(\omega_e t) \tag{9}$$

where $\mathrm{M_e} = 7.71 \times 10^{15}$ Wb.m is the magnetic dipole moment of Earth, $\varepsilon = 9.3^\circ$ is the magnetic dipole tilt angle, $\omega_\mathrm{e} = 7.29 \times 10^{-5}$ rad/s is the spin rate of Earth, and i is the orbit inclination. $\mathrm{c}(\cdot)$ and $\mathrm{s}(\cdot)$ are abbreviations for cosine and sine, respectively.

For the sun sensor, which is the other attitude sensor, the calibrated measurement model including sensor noise can be given as follows

$$\tilde{\boldsymbol{S}}_b = A\boldsymbol{S}_r + \boldsymbol{\eta}_s \tag{10}$$

where $\tilde{\boldsymbol{S}}_b$ is the measured sun direction vector in body frame, $\boldsymbol{S}_r$ is the sun direction vector in reference frame, and $\boldsymbol{\eta}_s$ is the sensor noise vector which is assumed to be a zero-mean white Gaussian noise. The sun direction vector $\boldsymbol{S}_r$ can be calculated via well-known sun direction calculation algorithms which one of them is presented in[22] and will not be repeated here for the sake of brevity.

Lastly, for the gyroscope, the measurement model including sensor noise and bias can be given as follows

$$\tilde{\boldsymbol{\omega}}_{bi} = \boldsymbol{\omega}_{bi} + \boldsymbol{\eta}_{\omega} + \boldsymbol{b}_{\omega} \tag{11}$$

where $\tilde{\boldsymbol{\omega}}_{bi}$ is the measured body angular velocity, $\boldsymbol{b}_{\omega}$ is the bias vector, and $\boldsymbol{\eta}_{\omega}$ is the sensor noise vector which is assumed to be a zero-mean white Gaussian noise. The behavior of gyroscope bias vector, on the other hand, is given by

$$\frac{d\boldsymbol{b}_{\omega}}{dt} = \boldsymbol{\eta}_{\omega,b} \tag{12}$$

where $\boldsymbol{\eta}_{\omega,b}$ is the bias noise vector which is assumed to be, again, a zero-mean white Gaussian noise.

3. TRIAD Algorithm

TRIAD algorithm (also known as the algebraic method or the two-vector algorithm) is one of the earliest published spacecraft attitude determination methods which requires two vector observations to fully determine the three-axis attitude[23]. Given two reference unit vector $\hat{\boldsymbol{V}}_1$, $\hat{\boldsymbol{V}}_2$ and measurement vectors $\widehat{\boldsymbol{W}}_1$, $\widehat{\boldsymbol{W}}_2$ corresponding to these reference vectors, the goal is to find an orthogonal attitude matrix A such that[24]

$$A\hat{\boldsymbol{V}}_1 = \widehat{\boldsymbol{W}}_1, \; A\hat{\boldsymbol{V}}_2 = \widehat{\boldsymbol{W}}_2 \tag{13}$$

Orthogonal attitude matrix A is known to be overdetermined, thus two triads of orthonormal reference and measurement vectors are constructed according to

$$\hat{\boldsymbol{r}}_1 = \hat{\boldsymbol{V}}_1 \tag{14}$$

$$\hat{\boldsymbol{r}}_2 = \left(\hat{\boldsymbol{V}}_1 \times \hat{\boldsymbol{V}}_2\right) / \left|\hat{\boldsymbol{V}}_1 \times \hat{\boldsymbol{V}}_2\right| \tag{15}$$

$$\hat{\boldsymbol{r}}_3 = \hat{\boldsymbol{r}}_1 \times \hat{\boldsymbol{r}}_2 \tag{16}$$

and

$$\hat{\boldsymbol{s}}_1 = \widehat{\boldsymbol{W}}_1 \tag{17}$$

$$\hat{\boldsymbol{s}}_2 = \left(\widehat{\boldsymbol{W}}_1 \times \widehat{\boldsymbol{W}}_2\right) / \left|\widehat{\boldsymbol{W}}_1 \times \widehat{\boldsymbol{W}}_2\right| \tag{18}$$

$$\hat{\boldsymbol{s}}_3 = \hat{\boldsymbol{s}}_1 \times \hat{\boldsymbol{s}}_2 \tag{19}$$

where there is a unique orthogonal matrix A which satisfies

$$A\hat{r}_i = \hat{s}_i, \qquad (i = 1,2,3) \tag{20}$$

Eq. (20) is known to be the TRIAD solution, and the necessary and sufficient condition for this solution to be valid is given as

$$\hat{\boldsymbol{V}}_1 \cdot \hat{\boldsymbol{V}}_2 = \widehat{\boldsymbol{W}}_1 \cdot \widehat{\boldsymbol{W}}_2 \tag{21}$$

Looking at Eq. (16) and Eq. (19), it is seen that part of the information contained in $\hat{\boldsymbol{V}}_2$ and $\widehat{\boldsymbol{W}}_2$ is discarded which causes TRIAD solution to be asymmetric. Therefore, in order to increase the accuracy of the algorithm, it is advised to choose the first vector observation to have the greater accuracy.

3.1. TRIAD Covariance Analysis

In order to compose the measurement noise covariance matrix (R) required for the Kalman filter, the covariance matrix of the attitude parameters obtained as a result of the TRIAD algorithm is needed. This covariance matrix can be calculated in terms of error angle vector elements as follows[24]

$$P_{\theta\theta} = \sigma_1^2 I_{3\times 3} + \frac{1}{\left|\widehat{\boldsymbol{W}}_1 \cdot \widehat{\boldsymbol{W}}_2\right|^2}\left[(\sigma_2^2 - \sigma_1^2)\widehat{\boldsymbol{W}}_1\widehat{\boldsymbol{W}}_1^T + \sigma_1^2\left(\widehat{\boldsymbol{W}}_1 \cdot \widehat{\boldsymbol{W}}_2\right)\left(\widehat{\boldsymbol{W}}_1\widehat{\boldsymbol{W}}_2^T + \widehat{\boldsymbol{W}}_2\widehat{\boldsymbol{W}}_1^T\right)\right] \tag{22}$$

It is also possible to write the covariance matrix given by Eq. (22) in terms of Euler angles (ϕ_1, ϕ_2, ϕ_3). The relationship between the two covariance matrices is given by

$$P_{\phi\phi} = HP_{\theta\theta}H^T \tag{23}$$

where the matrix H is calculated as follows

$$[H^{-1}]_{ij} = \frac{1}{2}\sum_{k=1}^{3}\left(\frac{\partial A_k}{\partial \phi_j} \times A_k\right)_i \tag{24}$$

where k represents the corresponding column of the attitude matrix A.

The attitude determination algorithm presented in this study uses quaternions as the attitude parameters. Therefore, a 4×4 covariance matrix is required for the determined quaternion set. This covariance matrix can be obtained using the 3×3 Euler angles covariance matrix given in Eq. (23) and well-known covariance law as follows[25]

$$P_{qq} = BP_{\phi\phi}B^T \tag{25}$$

where the matrix B is calculated as follows

$$B = \begin{bmatrix} \frac{\partial \phi_1}{\partial q_1} & \frac{\partial \phi_1}{\partial q_2} & \frac{\partial \phi_1}{\partial q_3} & \frac{\partial \phi_1}{\partial q_4} \\ \frac{\partial \phi_2}{\partial q_1} & \frac{\partial \phi_2}{\partial q_2} & \frac{\partial \phi_2}{\partial q_3} & \frac{\partial \phi_2}{\partial q_4} \\ \frac{\partial \phi_3}{\partial q_1} & \frac{\partial \phi_3}{\partial q_2} & \frac{\partial \phi_3}{\partial q_3} & \frac{\partial \phi_3}{\partial q_4} \end{bmatrix} \tag{26}$$

4. Extended Kalman Filter Formulation

The scheme for the TRIAD aided EKF algorithm for attitude, magnetometer bias, and gyro bias estimation is given in Figure 1, and the 10×1 state vector is presented as

$$\boldsymbol{x} = \begin{bmatrix} \boldsymbol{q} \\ \boldsymbol{b}_m \\ \boldsymbol{b}_{\omega} \end{bmatrix} \tag{27}$$

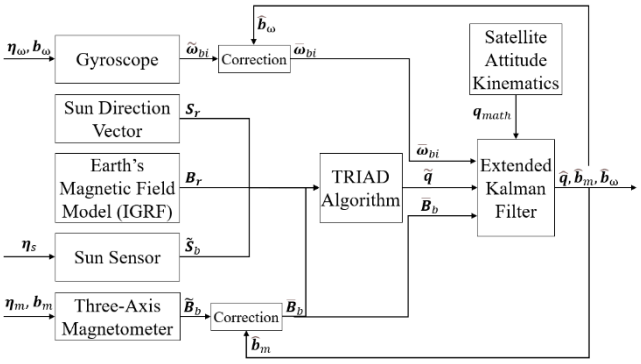

Fig. 1. Integrated TRIAD/EKF estimation system.

The state vector given in Eq. (27) can be propagated using the following discrete model[25]

$$\hat{\boldsymbol{x}}_{k+1}^{-} = \boldsymbol{f}(\boldsymbol{x}_k, k) + \boldsymbol{w}_k \tag{28}$$

where the function $\boldsymbol{f}(\boldsymbol{x}_k, k)$ is the nonlinear state transition function (maps the previous state to the current state), $\boldsymbol{w}_k$ is the process noise which is assumed to be a zero-mean white and Gaussian noise with the covariance of Q_k, and $\hat{}^{-}$ symbol represents the prediction.

The measurement vector for the filter consisting of TRIAD quaternion solution and magnetometer measurements is modeled as

$$\boldsymbol{z}_k = \boldsymbol{h}(\boldsymbol{x}_k, k) + \boldsymbol{v}_k \tag{29}$$

where the function $\boldsymbol{h}(\boldsymbol{x}_k, k)$ is the nonlinear measurement

model (maps the current state to the measurements) and $\boldsymbol{v}_k$ is the measurement noise which is, again, assumed to be a zero-mean white and Gaussian noise with the covariance of R_k. As can be clearly noticed, since the TRIAD quaternion solution ensures that attitude states are directly observable for the filter, parts corresponding to these states in the $\boldsymbol{h}(\boldsymbol{x}_k, k)$ function will become linear (identity matrix to be more precise). In this way, the necessity of Jacobian calculations for attitude states is eliminated when generating the predicted measurement vector.

On the other hand, the propagation of the state error covariance matrix P in discrete time is given by

$$\hat{P}_{k+1}^{-} = \Phi_k P_k \Phi_k^T + Q_k \tag{30}$$

where Φ_k is the state transition matrix and can be calculated by using the first-order Taylor series expansion at the sampling time T_s as follows

$$\Phi_k = e^{F_k T_s} \approx I + F_k T_s \tag{31}$$

where the matrix F_k is given by

$$F_k = \left.\frac{\partial \boldsymbol{f}(\boldsymbol{x}_k, k)}{\partial \boldsymbol{x}}\right|_{\boldsymbol{x}=\hat{\boldsymbol{x}}_k^+} \tag{32}$$

Eqs. (28) and (30) constitute the prediction part of the EKF which as a result, predictions are obtained. The correction (or update) part of the filter starts with calculating the Kalman gain matrix K_{k+1} as

$$K_{k+1} = \frac{\hat{P}_{k+1}^{-} H_{k+1}^T}{H_{k+1} \hat{P}_{k+1}^{-} H_{k+1}^T + R_{k+1}} \tag{33}$$

where H_{k+1} is known as the state observation matrix calculated as

$$H_{k+1} = \left.\frac{\partial \boldsymbol{h}(\hat{\boldsymbol{x}}_{k+1}^{-}, k+1)}{\partial \boldsymbol{x}}\right|_{\boldsymbol{x}=\hat{\boldsymbol{x}}_{k+1}^{-}} \tag{34}$$

After the calculation of the Kalman gain matrix, the correction is made for the predictions as

$$\hat{\boldsymbol{x}}_{k+1}^{+} = \hat{\boldsymbol{x}}_{k+1}^{-} + K_{k+1} \boldsymbol{y}_{k+1} \tag{35}$$

$$\hat{P}_{k+1}^{+} = (I - K_{k+1} H_{k+1}) \hat{P}_{k+1}^{-} \tag{36}$$

where $\boldsymbol{y}_{k+1}$ is known as the filter innovation (or residual) and defined as

$$\boldsymbol{y}_{k+1} = \boldsymbol{z}_{k+1} - \boldsymbol{h}(\hat{\boldsymbol{x}}_{k+1}^{-}, k+1) \tag{37}$$

5. Numerical Simulations and Discussion

In order to verify the performance of the proposed system various simulations are performed for a hypothetical nanosatellite. Table 1 shows the parameters for the numerical simulations including orbit and sensor specifications. Since direction cosines are used, there is no unit for the magnetometer and sun sensor specifications. It is also assumed that the satellite never enters eclipse throughout the orbit so that measurements are available from the sun sensor continuously.

Table 1. Simulation parameters (Std = Standard Deviation).

Angular velocity (rad/sec)	$(6.5, 6.6, 6.7)10^{-3}$
Altitude (km)	626
Orbital period (sec)	5833.7
Orbit eccentricity	0 (circular)
Orbit inclination (°)	111.5
Orbit right ascension (°)	15
Satellite moment of inertia $(kg \cdot m^2)$	$(2.1, 2.0, 1.9)10^{-3}$
Std of Sun sensor error	0.02
Std of magnetometer error	0.08
Std of gyroscope error (rad/sec)	0.001
Magnetometer bias vector	(0.2, 0.4, 0.6)
Gyroscope bias vector (rad/sec)	(0.58, 0.65, 0.73)

Figure 2, 3, and 4 show the estimation results using the above-mentioned parameters. Looking at figures, it is seen that the filter needs approximately 1000 seconds to converge which is nearly $1/6^{th}$ of one full orbit. In order to understand the accuracy of the estimations better, Table 2 shows root mean square errors (RMSEs) for each state after the filter convergence. Since most of the processes in the system are stochastic, 100 Monte Carlo runs are executed and RMSE values are calculated by taking the average of these runs.

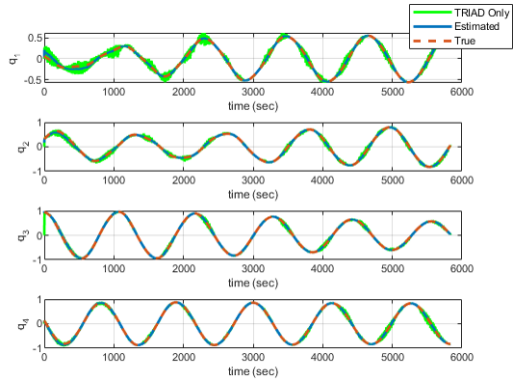

Fig. 2. Attitude estimation results (quaternions).

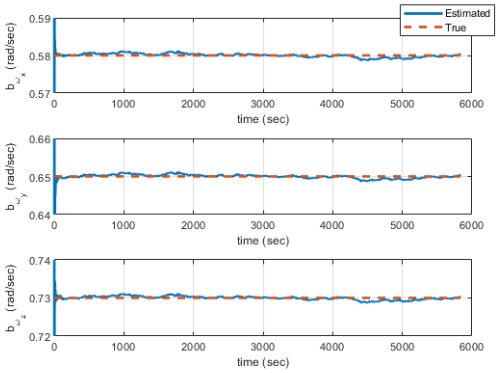

Fig. 3. Gyro bias estimation results.

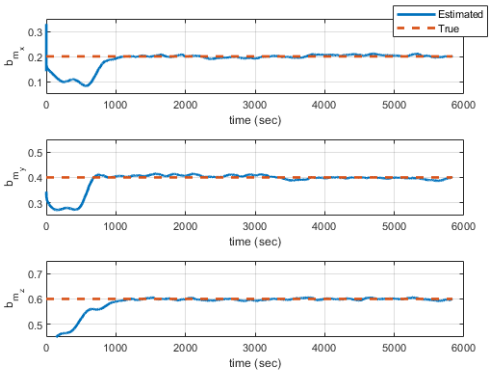

Fig. 4. Magnetometer bias estimation results.

Table 2. RMSE values for each state (100 Monte Carlo run).

States	RMSE Value
$\boldsymbol{q_1}$	0.004729
$\boldsymbol{q_2}$	0.004999
$\boldsymbol{q_3}$	0.004040
$\boldsymbol{q_4}$	0.004462
b_{m_x}	0.005362
b_{m_y}	0.007085
b_{m_z}	0.003949
$b_{\omega_x}(rad/sec)$	0.000422
$b_{\omega_x}(rad/sec)$	0.000267
$b_{\omega_x}(rad/sec)$	0.000439

Simulations are also performed in different angular velocities to observe the behavior of the system. Table 3 shows the RMSE values for states in three different satellite angular velocities. In Table 3, angular velocity vectors are presented as $0.1\boldsymbol{\omega}$, $\boldsymbol{\omega}$, and $10\boldsymbol{\omega}$ representing the multiples of the angular velocity value ($\boldsymbol{\omega}$) given in Table 1. For example, $10\boldsymbol{\omega}$ corresponds to an angular velocity vector of $(6.5,6.6,6.7)10^{-2}$ rad/sec. When the results are examined, it is seen that the accuracy of attitude and magnetometer bias estimations increases when the initial angular velocity vector of the satellite is increased. However, a similar consistent trend in gyroscope bias estimations is not observed. Improvement in some estimations due to the increase in the angular velocity vector is an expected thing since Kalman filters are generally known to work better in dynamical systems than in stationary systems.

Table 3. RMSE values in different angular velocities (100 Monte Carlo run).

States	Angular Velocity ($\boldsymbol{\omega}$)		
	$0.1\boldsymbol{\omega}$	$\boldsymbol{\omega}$	$10\boldsymbol{\omega}$
	RMSE Values		
$\boldsymbol{q_1}$	0.010834	0.004729	0.002836
$\boldsymbol{q_2}$	0.022945	0.004999	0.003053
$\boldsymbol{q_3}$	0.003294	0.004040	0.002750
$\boldsymbol{q_4}$	0.10162	0.004462	0.002811
b_{m_x}	0.032073	0.005362	0.002081
b_{m_y}	0.022561	0.007085	0.002331
b_{m_z}	0.031748	0.003949	0.002124
$b_{\omega_x}(rad/sec)$	0.000355	0.000422	0.000356
$b_{\omega_x}(rad/sec)$	0.000447	0.000267	0.000280
$b_{\omega_x}(rad/sec)$	0.000374	0.000439	0.000349

Lastly, in order to test the performance of the proposed system in case of time-varying magnetometer bias, two additional simulations are performed. These simulations include a time-varying sinusoidal bias and a bias where there is an active bias drift. Figure 5 and 6 show the bias estimation results.

Looking at Figure 5 and 6 it is seen that the proposed system can also successfully estimate various types of time-varying magnetometer biases. In addition to figures, Table 4 shows the RMSE values of the estimations for different type of magnetometer biases including the constant bias case given by Figure 4 and Table 2.

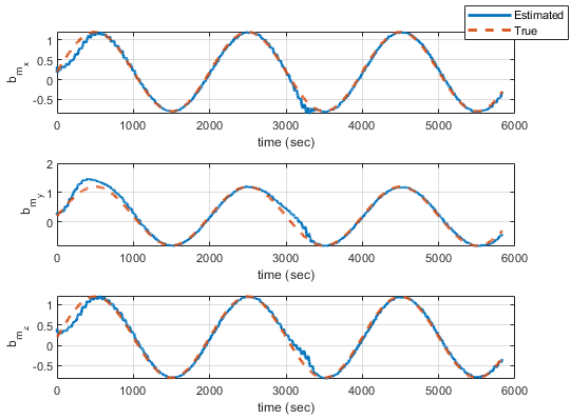

Fig. 5. Magnetometer bias estimation results in case of sinusoidal bias (0.0005 Hz frequency).

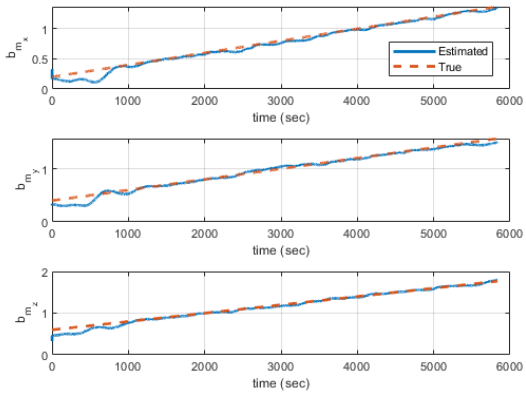

Fig. 6. Magnetometer bias estimation results in case of bias drift (0.0001 drift rate).

Table 3. RMSE values for different types of magnetometer biases (100 Monte Carlo run).

States	Magnetometer Bias Type		
	Constant	Sinusoidal	Drift
	RMSE Values		
$\boldsymbol{q_1}$	0.004729	0.007555	0.005486
$\boldsymbol{q_2}$	0.004999	0.008712	0.006335
$\boldsymbol{q_3}$	0.004040	0.007248	0.005640
$\boldsymbol{q_4}$	0.004462	0.007199	0.005367
b_{m_x}	0.005362	0.026835	0.022742
b_{m_y}	0.007085	0.029254	0.023304
b_{m_z}	0.003949	0.026348	0.022509
$b_{\omega_x}(rad/sec)$	0.000422	0.001049	0.000892
$b_{\omega_x}(rad/sec)$	0.000267	0.001020	0.000912
$b_{\omega_x}(rad/sec)$	0.000439	0.001093	0.000936

Looking at Table 4, it is seen that the proposed system gives the best results in the presence of a constant magnetometer bias vector. The accuracy of the estimations is partially reduced when the type of bias is time-varying. At the same time, it is observed that the system gives more accurate results in the case of bias drift compared to the sinusoidal bias.

6. Conclusion

In this study, a nontraditional small satellite attitude estimation system based on the TRIAD algorithm and an extended Kalman filter (EKF) is proposed. The TRIAD algorithm is used as the first phase attitude determination algorithm and obtained estimation is given to the EKF as input together with the angular velocity measurements provided by the gyroscope. In order to increase the accuracy of the attitude estimation, the proposed system also calibrates the magnetometer and gyroscope biases simultaneously. The performance of the system is tested via several simulations. In the first simulation, general performance of the system is verified where constant bias vectors are applied to the magnetometer and the gyroscope. On the other hand, in the second simulation, the performance of the system is tested in different satellite angular velocities and a trend is observed that the attitude and magnetometer bias estimations improved with increasing angular velocity. However, this does not apply to gyroscope bias estimation. For this reason, it is recommended to investigate the relationship between angular velocity and gyroscope bias estimation in more detail in future studies. Lastly, in the third simulation, the proposed system is tested against two different time-varying magnetometer bias vectors, as one being the sinusoidal bias and the other one being the presence of bias drift. The third simulation results show that the system is also capable of estimating various types of time-varying magnetometer biases, although the estimation accuracy reduces slightly.

References

1. Poghosyan, A. and Golkar, A.: CubeSat evolution: Analyzing CubeSat capabilities for conducting science missions, Progress in Aerospace Sciences, Vol. 88, 2017, pp. 59-83.
2. Tafazoli, M.: A study of on-orbit spacecraft failures, Acta Astronautica, Vol. 64, Issues 2-3, 2009, pp. 195-205.
3. Lefferts, E., Markley, F., and Shuster, M.: Kalman filtering for spacecraft attitude estimation, Journal of Guidance, Control, and Dynamics, Vol. 5, No. 5, 1982, pp. 417-429.
4. Sekhavat, P., Gong, Q., and Ross, I.M.: NPSAT1 parameters estimation using unscented Kalman filtering, In 2007 American Control Conference, 2007, pp. 4445-4451.
5. Springmann, J.C. and Cutler, J.W.: Flight results of a low-cost attitude determination system, Acta Astronautica, Vol. 99, 2014, pp. 201-214.
6. Psiaki, M.L., Martel, F., and Pal, P.K.: Three-axis attitude determination via Kalman filtering of magnetometer data, Journal of Guidance, Control, and Dynamics, Vol. 13, No. 3, 1990, pp. 506-514.
7. de Oliveira, G.F. et al.: A low-cost attitude determination and control system for the UYS-1 nanosatellite, In 2013 IEEE Aerospace Conference, 2013, pp. 1-14.
8. Hajiyev, C. and Bahar, M.: Attitude determination and control system design of the ITU-UUBF LEO1 satellite, Acta Astronautica, Vol. 52, No. 2, 2003, pp. 493-499.
9. Ainscough, T., Zanetti, R., Christian, J., and Spanos, P.D.: Q-method extended Kalman filter, Journal of Guidance, Control, and Dynamics, Vol. 38, No. 4, 2015, pp. 752-760.
10. Kinatas, H. and Hajiyev, C.: QUEST Aided EKF for attitude and rate estimation using modified Rodrigues parameters, WSEAS Transactions on Systems and Control, Vol. 17, pp. 250-261.
11. Hajiyev, C., Cilden, D., and Somov, Y.: Integrated SVD/EKF for small satellite attitude determination and rate gyro bias estimation, IFAC-PapersOnLine, Vol. 48, No. 9, 2015, pp. 233-238.
12. Markley, F. and Crassidis, J.: Fundamentals of Spacecraft Attitude Determination and Control, Springer Science+Business Media, New York, NY, 2014.
13. Soken, H.E.: A survey of calibration algorithms for small satellite magnetometers, Measurement, Vol. 122, 2018, pp. 417-423.
14. Forno, R.D. et al.: Autonomous navigation of MegSat1: Attitude, sensor bias and scale factor estimation by EKF and magnetometer-only measurement, In 22nd AIAA International Communications Satellite Systems Conference (ICSSC), 2004.
15. Soken, H.E. and Hajiyev, C.: UKF-Based reconfigurable attitude parameters estimation and magnetometer calibration, IEEE Transactions on Aerospace and Electronic Systems, Vol. 48, No. 3, 2012, pp. 2614-2627.
16. Inamori, T. et al.: Online magnetometer calibration in consideration of geomagnetic anomalies using Kalman filters in nanosatellites and microsatellites, Journal of Aerospace Engineering, Vol. 29, No. 6, 2016.
17. Hajiyev, C. and Soken, H.E.: Fault Tolerant Attitude Estimation for Small Satellites, Crc Press Taylor & Francis Group, Boca Raton, FL, 2021.
18. Kim, O.J. et al.: In-orbit results and attitude analysis of the SNUGLITE cube-satellite, Applied Sciences, Vol. 10, No. 7, 2020.
19. Soken, H.E. and Sakai, S.I.: TRIAD+Filtering approach for complete magnetometer calibration, In 2019 9th International Conference on Recent Advances in Space Technologies (RAST), 2019, pp. 703-708.
20. Soken, H.E.: An attitude filtering and magnetometer calibration approach for nanosatellites, International Journal of Aeronautical and Space Sciences, Vol. 19, pp. 164-171.
21. Thébault, E. et al.: International geomagnetic reference field: the 12th generation, Earth, Planets and Space, Vol. 67, 2015.
22. Vallado, D.: Fundamentals of Astrodynamics and Applications, Microcosm Press, Hawthorne, CA, 4th edition, 2013.
23. Black, H.D.: A passive system for determining the attitude of a satellite, AIAA Journal, Vol. 2, No. 7, 1964, pp. 1350-1351.
24. Shuster, M.D. and Oh, S.D.: Three-axis attitude determination from vector observations, Journal of Guidance and Control, Vol. 4, No. 1, 1981, pp. 70-77.
25. Crassidis, J. and Junkins, J.: Optimal Estimation of Dynamic Systems, Crc Press Taylor & Francis Group, Boca Raton, FL, 2nd edition, 2012.